**PAPER**

Check for updates

# A self-healable metallohydrogel for drug encapsulations and drug release†

Mita Dutta, [ID] [a] Shreya Banerjee,[b] Mahitosh Mandal[b] and Manish Bhattacharjee [ID] *[a]

A self-healable metallohydrogel (MOG) of Mn(II) has been prepared using a low molecular weight gelator, Na$_2$HL {H$_3$L = L-(3,5-di-*tert*-butyl-2-hydroxy-benzyl)amino aspartic acid}. The MOG has been characterized by MALDI TOF mass spectrometry, rheological studies, IR spectroscopy, and microscopic techniques. Non-steroidal anti-inflammatory drug (NSAID), indomethacin (IND) and anti-cancer drug gemcitabine (GEM) were encapsulated into the metallohydrogel. The GEM-loaded metallogel (MOG_GEM) shows better delivery and more adverse cytotoxicity than the drug against breast cancer cell lines MDA-MB-468 and 4T1. The anti-cancer property was evaluated with *in vitro* MTT cytotoxic assay, live-dead assay and cell migration assay. *In vitro* cytotoxicity assay against RAW 264.7 cell line with the treatment of MOG_IND shows the improved anti-inflammatory response in the case of MOG_IND compared to the drug alone.

## Introduction

In recent years, the development of smart materials has gained importance. One of the major areas is the synthesis of low molecular weight gelators (LMW) and their use in synthesizing metal–organic gels.[1–7] A large amount of solvent is immobilized in a 3D cross-linked network.[8,9] Gels are produced primarily *via* non-covalent interactions, which is evident from the structural reversibility under various mechanical and thermal conditions. Adding a metal ion to the gel matrix with the gelator molecule imparts specific properties of the metal ion into the gel network. The metal–organic gels have been used in catalysis,[10] adsorption of toxic substances,[11] and in the preparation of materials for electronics,[12,13] sensors,[14,15] light emitting materials,[16,17] and drug delivery systems.[18–22] Metal–ligand coordination complexes and coordination polymers have been reported to generate metallogels, which occasionally contain metal nanoparticles.[23–25]

In the past few decades, substantial progress has been made in the drug development and technology for cancer treatment. Cancer remains a serious public health issue and one of the world's top causes of death.[26] Among the currently available therapies (surgery, radiotherapy, chemotherapy, hormone therapy, immunological therapy, gene therapy, targeted therapy), each has its drawbacks.[27] Chemotherapy is the most effective treatment method to eradicate cancer cells.

Chemotherapy uses cytotoxic chemicals.[28] Delivering therapeutic agents to the channel is the most significant hurdle for cancer treatment. Typically, the drug is placed into a carrier medium and transported to the desired spot.[18] It is important to mention that drug distribution is a significant phenomenon that affects the pharmacokinetics, rate of release, duration, and after-release side effects.[29,30] It is challenging to develop a drug delivery system (DDS), keeping all these in mind.[31] Many drug delivery systems are being used clinically to deliver a wide range of chemotherapeutic medications.[28] Existing drug delivery methods include dendrimers,[32] liposomes,[33] metal nanoparticles,[34] and polymers,[35] among others.[30,36] Although significant advancements have been made in recent years, challenges still exist. Several of these DDS are not biodegradable or have other problems, like loading efficiency, poor bioavailability, high-dose requirements, and local irritation.[37] Recently, inorganic and organic hybrid systems (IOHs), such as coordination polymers and coordination complexes have been used as drug delivery systems.[38] Since then, there has been worldwide interest in developing IOHs based DDS.[38–41] These IOHs have the advantages of larger drug loading capacity and the elimination of unintended side effects. There are reports on DDS based on metallogels. A copper-based metallogel has been developed by Choudhary *et al.* for the delivery of an anti-inflammatory drug.[31] Sarkar *et al.* reported silver and manganese-based metallogel involving hydrogen bond functionalized ligands and employed it as self-deliverable DDS.[40] Another group recently reported a series of metallogels. Among them, Zn(II) based metallogel was suggested to be active as a potential material in treating post-operative cancer surgery.[42]

Drug-loaded gels have several advantages over the drug alone, including better control over drug release, better

*[a]Department of Chemistry, Indian Institute of Technology, Kharagpur 721302, India. E-mail: mxb@iitkgp.ac.in*

*[b]School of Medical Science and Technology, Indian Institute of Technology, Kharagpur, 721302, India*

targeting of the affected tissue, and increased bioavailability. These factors can lead to improved therapeutic performance.[52] Supramolecular gels are made up by physically cross-linked weak and highly dynamic host–guest complexations. This type of network increases drug efficacy and maximising patient compliance. Also, the highly dynamic network of hydrogels allows injection of encapsulated drugs, thereby simplifying administration during surgery.[53]

Drug-loaded gel can control the cell migration by releasing the drug into the extracellular matrix (ECM) around cells.[54] Drug or drug-loaded can degrade or modify the stiffness or permeability of the ECM surrounded cell. This alteration can affect cell migration, as cells can sense the stiffness and porosity of their surroundings and adjust their behaviour accordingly. Another way the drug-loaded hydrogels can influence cell migration is by affecting intracellular signaling pathways. Many drugs can bind to specific receptors on the cell surface or penetrate into the cell, affecting various signaling pathways. These pathways regulate cell behaviour, including migration.

Controlled mixing of a gelator, an ion, solvent, and a drug produces robust material with a long-time release profile in the physiological environment. With this background, we thought of using metallogels for drug loading and delivery.

Previously, we have explored the gelation ability with some first-row transition metal ions, like Cu(II) and Zn(II). The Cu(II) MOG was used as a catalyst for the fixation of $CO_2$ and $SO_2$.[43a] The Zn(II) MOG was used as a gel electrolyte to fabricate a supercapacitor.[43b] We have reported the synthesis of self-healable $Co^{2+}$, $Ni^{2+}$, and $VO^{2+}$ gels using the gelator, L-(3,5-di-*tert*-butyl-2-hydroxy-benzyl)amino aspartic acid [Na$_2$HL]. The Co(II) and the Ni(II) gels were found to absorb selectively cationic dyes from dye mixtures.[43c] A few years back we reported preparation of Zn(II) and Cd(II) gels using disodium salt of the ligand carboxymethyl-(3,5-di-*tert*-butyl-2-hydroxy-benzyl)amino acetic acid. These gels show self-healing property. These gels were shown to be reusable materials for selective dye adsorption.[44a] The same ligand was used for the synthesis of a Cu(II) gel, which acts as a catalyst for CuAAC reaction and fixation of $CO_2$.[44b] In continuation of the works, herein we report the synthesis of manganese(II) based metallogel, using the disodium salt of the ligand, L-(3,5-di-*tert*-butyl-2-hydroxy-benzyl)amino aspartic acid [Na$_2$HL]. The metalorganic gel shows self-healing properties. This gel has been used as an *in vitro* drug delivery agent for two drugs, gemcitabine (GEM), a drug used to treat ovarian cancer, and indomethacin (IND), an NSID (Fig. 1).

# Results and discussion

Amino acid-based ligands can form metal–organic gels with several metal ions.[46] Among various metal ion Mn(II) based gel has been shown to be biocompatibile.[40,47] With this inspiration in mind, we have synthesized an Mn(II) based metallohydrogel (MOG) with the ligand, Na$_2$HL, reported from this laboratory (Scheme 1). The gelator (ligand) molecule contains aspartic acid with two strategically carboxylate groups and one amine group. These are the active site to bind with metal ions. The ligand, Na$_2$HL, comprises two active carboxylate groups, one –NH– group and a phenolic group. The –NH–CH–COO group is ideally deposed for binding the metal. The rest of the groups are used to form hydrogen bonding with solvent water molecules, which is responsible for forming metal–organic gel (Scheme 1). It may be noted that in the MALDI-TOF spectrum, we could see the peak for the 1 : 1 complex of $Mn^{2+}$ ion and the ligand (*vide infra*).

The metallohydrogel was prepared by mixing aqueous solutions of Mn(II) salt and the gelator in a 1 : 1 ratio at room temperature. To further understand the minimum concentration of metal and the ligand for the gelation, we took five solutions of different concentrations, starting from 0.01 mole to 0.05 mole (Fig. S1, ESI†). A stable pale pink metallohydrogel was obtained at 0.01 mole concentration. The minimum gelation concentration (MGC) of the MOG is 2.3 wt%. As we increase the concentration beyond MGC, we get the opaquer gel. The colour of the gel arises due to the ligand-to-metal charge transfer.

The gel is thermos and mechano reversible. With increasing temperature, the gel starts converting into the sol, while decreasing the temperature results in gel formation (Fig. S2; ESI†). The external mechanical force (*e.g.*, shaking by hand) converts the gel into sol. The sol converts back into the gel when left undisturbed at room temperature.

The gel is highly stable at room temperature and could not get any phase separation for more than six months in a sealed vial. After the formation of the MOG, two drugs, gemcitabine (MOG-GEM) and indomethacin (MOG-IND), were encapsulated in the gel. Samples of 5 mg of each drug were separately incorporated into the MOG (Scheme 2).

The MOG and the drug-incorporated MOGs were characterized by MALDI-TOF, IR spectroscopy,[48,49] and rheological and microscopic studies. The MALDI-TOF spectrum of the MOG shows peaks at $m/z = 373.55$, which corresponds to the molecular weight of the gelators + $H^+$ (calculated $m/z = 374.19$)
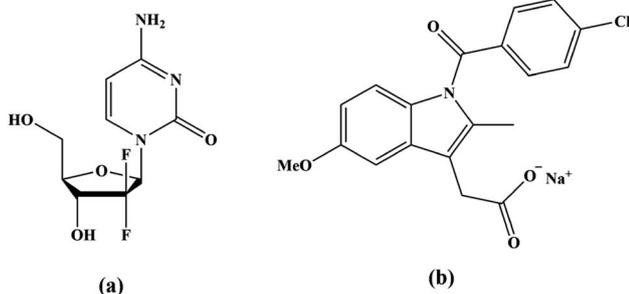


**Fig. 1** Structure of the (a) gemcitabine and (b) sodium salts of indomethacin.
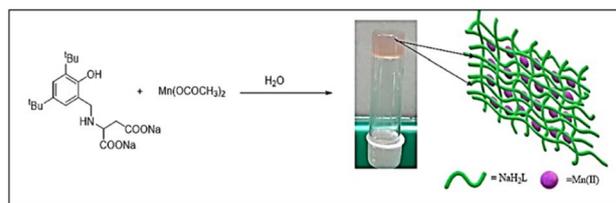


**Scheme 1** Schematic representation of the synthesis of the MOG.
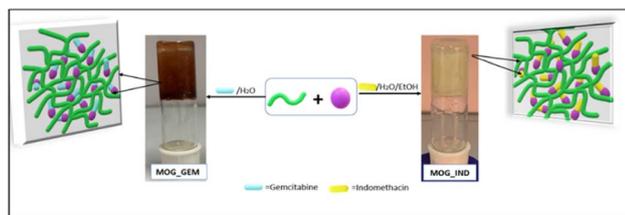
**Scheme 2** Schematic representation of drug encapsulation into the bulk gel.



**Fig. 3** Frequency sweep of the (a) MOG (b) MOG_IND (c) MOG_GEM.

and $m/z = 421.79$, which corresponds to a 1 : 1 complex of the mono anion of the ligand and $Mn^{2+}$ along with a water molecule (calculated $m/z = 422.14$) (Fig. S4 and S5; ESI†). Thus, we suggest the presence of a 1 : 1 metal–ligand complex in the gel matrix (Fig. 2).

We have investigated the structure of the drug-loaded xerogels with powder X-ray diffraction experiments (Fig. S6; ESI†). The appearance of the first peak at $2\theta = 10.5°$, corresponds to the (001) plane indicated interlayer spacing of graphite oxide like structure.[50] The second broad peak at $2\theta = 24.79°$ is associated with the (002) plane of the carbon support.[51] The overall broad spectrum in PXRD revealed the amorphous nature of the drug encapsulated xerogel.

The MOG is stable in the pH range of 4 to 8. When hydrochloric acid (pH below 4) was added to the MOG, we obtained a clear solution with some white residue due to the precipitation of the ligand. Thus, the MOG is pH responsive. When an aqueous solution [0.1(M)] of EDTA was added, we obtained a solution with the white precipitate of the ligand (Fig. S2, ESI†). Next, we added a few drops of aqueous ammonia to the gel's surface and obtained a brown precipitate. The precipitate is due to the formation of $Mn(OH)_2$, which was easily oxidized by atmospheric oxygen to form $MnO(OH)$. The same result was obtained at higher pH < 8 when the gel was treated with NaOH solution.

The mechanical strength of the gel is critical since it can define how stiff the gel should be for its use. The rheological investigation was carried out to investigate the mechanical

properties of the gel and the drug-loaded gels. Fig. 3 displays the results of the frequency sweep and Fig. 4 shows the results of step-strain experiments. Fig. S8† (ESI) displays the results of the amplitude sweep experiment of the MOG, MOG_IND, and MOG_GEM. Frequency sweep experiment was conducted with 0.5% strain. The average storage modulus (G′) was found to be larger than the loss modulus (G″) throughout the experiment. The storage modulus (G′) of the MOG was found to be 17 174 Pa. This result demonstrates that the MOG is more elastic than viscous. Drug-incorporated gels' mechanical characteristics differ from those of a pure metallohydrogel. For MOG_IND and MOG_GEM, the average G′ was found to be 32 821 Pa and 16 303 Pa, respectively. The amplitude sweep experiments (Fig. S7; ESI†) show that the cross-over points for the MOG, MOG_IND, and MOG_GEM are 292 Pa, 261 Pa and 714 Pa, respectively. In the step-strain experiment, at the highest strain (100%), G′ and G″ reduced, reflecting the gel's deformation. When the strain was reduced to 0.1%, rapid recovery of nearly 100% of the original modulus value was noticed for three cycles, demonstrating that the gel had returned to its initial state (Fig. 4). The results were consistent with the self-healing (thixotropy) property of the metallohydrogel. We have also carried out frequency sweep experiment of the gel at 2% strain (Fig. S8; ESI†). The nature of the of the curves does not change. The average distance between the storage and loss moduli is 9918 Pa, which is considerably less than the prior value of 17 174 Pa. Therefore, we can argue that gel elasticity decreases as strain increases.

We examined the rheological characteristics of the pristine gel and the self-healed gel, separately while maintaining the same settings (Fig. S9; ESI†). The cross-over point of healed



**Fig. 2** FT IR spectra of the MOG, MOG_IND and MOG_GEM.
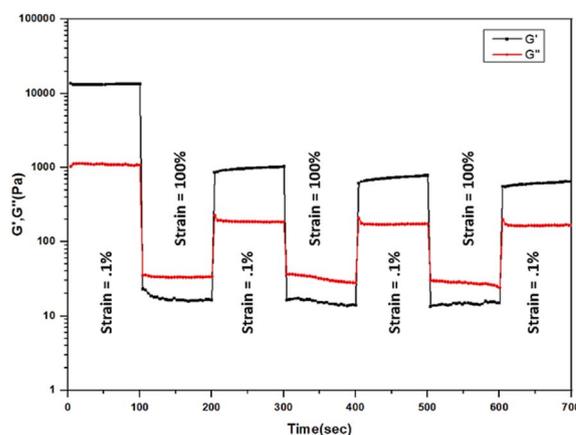


**Fig. 4** Step-strain experiment of the MOG.
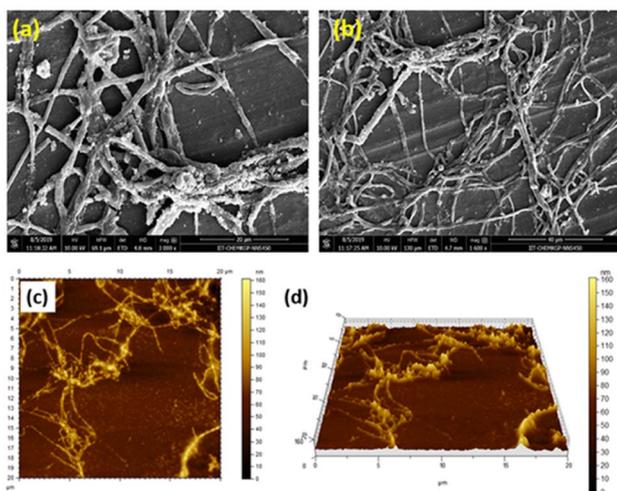
**Fig. 5** FESEM images of the MOG at (a) 20 μm, (b) 40 μm. AFM images (c and d) of the MOG.

MOG is 626 Pa. Hence, the healed gel deforms somewhat less shear stress region than the pristine gel. However, a frequency sweep experiment showed that the average $G'$ and $G'$ values for the healed gel are higher than those for the pristine gel. It indicates that after healing, the gel's elasticity has risen.

The morphological analyses by the field-emission scanning electron microscopy (FESEM) demonstrate that the MOG has a fibrous structure (Fig. 5a and b). The atomic force microscopic (AFM) images also show the fibrous nature of the MOG (Fig. 5c and d). The AFM images were recorded applying the spin coating technique. The TEM images of the MOG confirm the fibrous nature of the MOG. Several micrometer-sized cyclic networks made up of fibres were visible in the tunnelling electron microscopic (TEM) images of the MOG (Fig. 6a–c), resembling natural macromolecular hydrogel structure. The size of the cyclomer in TEM images suggests that the gel network has different sizes of pores. The thickness of the cellular pore walls lies in the range of 34 nm to 50 nm.

The FESEM images of the drug-loaded MOGs reveal presence of dense, highly aggregated multi-joined poly-dispersed fibres (Fig. 7a and b). Which indicates the significant interaction among the drug molecule, metal and the ligand present. The
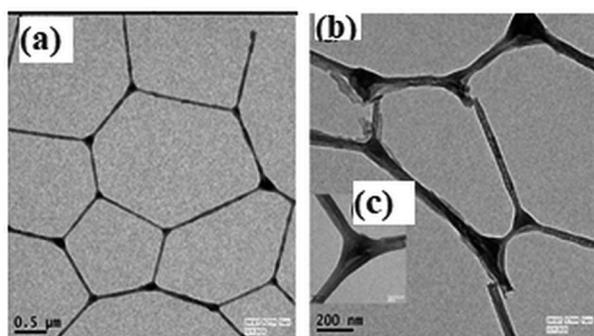


**Fig. 6** TEM images of the MOG at (a) 500 nm, (b) 200 nm, and (c) 50 nm.
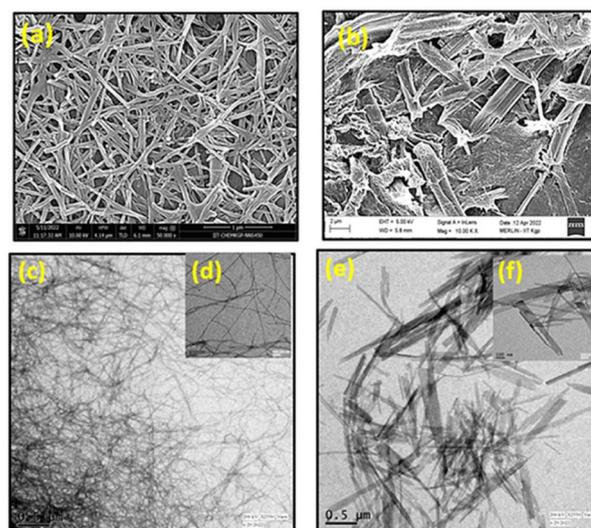


**Fig. 7** FESEM images of (a) MOG_GEM (scale 1 μm) and (b) MOG_IND (scale 2 μm). TEM images of (c) and (d) MOG_GEM (scale 0.5 μm and 100 nm respectively); (e) and (f) MOG_IND (scale 0.5 μm and 100 nm respectively).

TEM images of the drug loaded gels show significant aggregation within the fibres (Fig. 7c–f).

The AFM images of the MOG_GEM (Fig. 8a, b) and MOD_IND (Fig. 8c, d) also show the similar aggregated fibril network of the drug-loaded gels which is consistent with the other microscopic data.

We also examined the self-healing property of the MOG. We prepared four gel blocks of the MOG (Fig. 9a) and kept them in contact with each other without any external force. A few minutes later, four blocks shelf-healed together by forming a single block (Fig. 9b and c). Also, a dye doped MOG block was prepared with Rhodamine B and constructed a bridge (Fig. S10, ESI†) with dye doped and undoped MOG blocks for the better visualisation of the self-healing property. These experiments prove the reversible cross-linking into the gel matrices. Further,
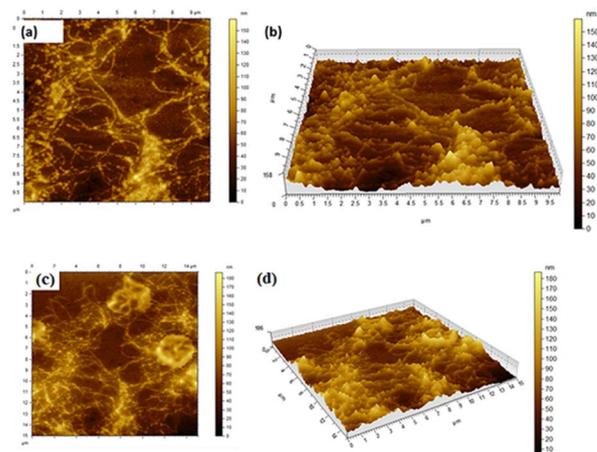


**Fig. 8** AFM images of (a), (b) MOG_GEM (scale 1 μm), (c) and (d) MOG_IND.
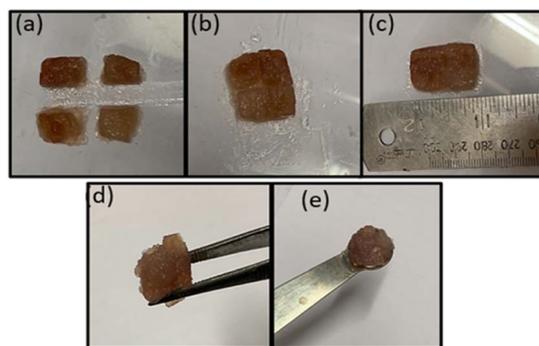
Fig. 9    Self-healing and self-sustaining properties of the MOG.



Fig. 11    Cytotoxicity study in the (a) 4T1 and (b) MDA–MB–468 cell by MTT assay.

the MOG can easily be held by a spatula and forceps (Fig. 9d and e). That is, the MOG has self-sustaining property.

Next, we examined the drug release from the drug-loaded MOG, MOG_GEM. The studies were carried out at two different pH, 7.4 and 5.8, at 37 °C. The amount of drug released was determined based on the total weight of the gel utilized. UV-visible spectroscopy was used to monitor the release of the anticancer drug from the bulk gel of MOG_GEM after interpolation from previously standardized UV-visible spectrophotometry calibration curves for MOG and drug.

The applicability of the drug-loaded metallohydrogels for drug delivery was evaluated with MOG_GEM and MOG_IND. Fig. 10 shows the % release of the drug *versus* time. After 48 hours, approximately 50% of the drug release was observed for MOG_GEM. Similarly, in the case of MOG_IND, about 60% drug release was observed in 50 hours at pH 5.8 (Fig. S11, ESI†).

We studied the potential biomedical uses of MOG_IND and MOG_GEM. The cytotoxicity of MOG_GEM on breast cancer cell line (4T1 & MDA-MB-468) was determined by MTT assay. Cells were treated with MOG_GEM, GEM, MOG for 48 hours to check the cytotoxicity of the compounds. As seen in Fig. 11, $IC_{50}$ value of MOG_GEM in different breast cancer cell lines (4T1: 3 μg ml$^{-1}$; MDA-MB-468: 5.50 μg ml$^{-1}$) were significantly lower compared to the drug alone (GEM) ($IC_{50}$: 4T1: 7.95 μg ml$^{-1}$, MDA-MB-468: 64.05 μg ml$^{-1}$). Besides, metallohydrogel (MOG)

alone did not show any significant cytotoxicity. The $IC_{50}$ value of MOG was found to be quite high compared to MOG_GEM ($IC_{50}$:4T1: 120.45 μg ml$^{-1}$, MDA-MB-468: 96 μg ml$^{-1}$). The MTT assay results indicates that the MOG_GEM may have a better inhibitory effect on tumour proliferation.

We also tested the cytocompatibility of the MOG and MOG_GEM by incubating them with L929 cell culture. Cells that had not been treated served as standard control. We conducted the MTT assay with the same dose range of these compounds for 48 h. It was found that the compounds do not show any significant cytotoxicity as the $IC_{50}$ was very high in L929 cells ($IC_{50}$: MOG_GEM: 84 μg ml$^{-1}$) (Fig. S12, ESI†).

The anti-inflammatory response of indomethacin-encapsulated MOG was tested for its cytotoxicity against RAW 264.7 cells using the MTT assay. The data shows that MOG_IND is biocompatible and is significantly better than IND alone ($IC_{50}$ = 15.62 μg ml$^{-1}$ for MOG_IND, 31.25 μg ml$^{-1}$ for IND) (Fig. S13, ESI†).

To revalidate the results obtained from the MTT assay, we performed a live-dead assay with calcein AM and propidium iodide. When the cells were treated with the calcein AM stain, the live cells appeared green under the fluorescent microscope, whereas dead cells appeared red after treatment with propidium iodide. High numbers of live cells are seen under the microscope in the control set of both 4T1 and MDA-MB-468 cell lines. In the cases of MOG, only a few numbers of dead cells are seen (Fig. 12). When the cell lines were treated with MOG_GEM and GEM, respectively, for 24 hours, very high numbers of dead cells were found where the cells appeared round, indicating



Fig. 10    Release of Gem from MOG_Gem monitored by UV-visible spectroscopy (a) $T$ = 48 hours (b) $T$ = 4 hours.
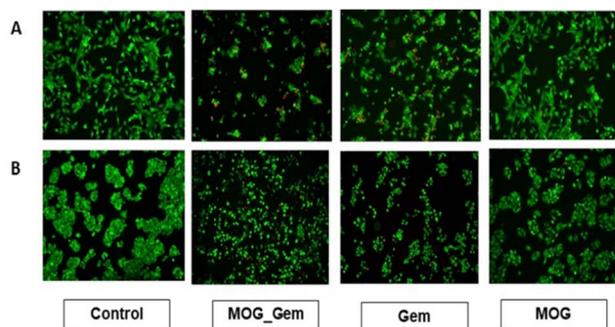


Fig. 12    Live dead assay of (A) 4T1 and (B) MDA–MB–468 cell after treatment with MOG_GEM, GEM, MOG.

dead cells. It is clear from Fig. 12 that cell morphology has changed most adversely after the treatment of MOG_GEM. Live dead assay of MDA-MB-468 after 48 hours of treatment is given in Fig. S14 (ESI†), where red stain could be seen clearly.

Regular cell migration is an action that is crucial to the growth and upkeep of multicellular organisms. However, unchecked and intentional migration causes metastasis in cancer cells. Consequently, a method for evaluating a compound's anti-cancer properties is the cell migration assay. Untreated control cells and cells treated with only metallohydrogel have shown very high migratory potential among all four different sets. On the contrary, MOG_GEM-treated cells have shown the lowest migratory potential (Fig. 13), which correlates with the MTT and live-dead assay data. Moreover, GEM-treated cells have shown intermediate migratory potential among different cells after 48 h of incubation. Migration speed topical showed that MOG_GEM most efficiently delayed the cells' movement, exhibiting effective anti-cancer activity (*in vitro*).

Due to the presence of metal salt in MOG_GEM, the metal may be hazardous. If metal salt is supplied intravenously or through the muscles, there may be substantial toxicity. On the other hand, topical *in vivo* application is anticipated to dramatically lower the toxicity as it is now placed locally on the target site and permeate through numerous barriers (skin, veins, *etc.*) to reach the bloodstream. Additionally, the metal ion concentration must be adjusted before real-world applications to lower the toxicity level to an acceptable range. Commercially available metal-containing formulations for treating inflammation, infection, and burn wounds include concentrated $Zn(NO_3)_2$ solution for treating gum inflammation, $AgNO_3$ in gel matrix for preventing secondary infection in cut injuries, and mafenide acetate cream for the treatment of burn wounds. The

current effort could be seen as a proof-of-concept to provide a strategy for treating cancer. Thus, the concern about toxicity induced by the ingredient (the metal salt) should be handled accordingly in the light of the pertinent discussion given above. MOG, as well as the drug-encapsulated MOGs, show good mechanical strength. The MOG is biocompatible.

## Conclusions

A new MOG containing Mn(II) ion and amino acid-based gelator has been synthesized. The MOG shows self-sustainability and self-heal ability. The MOG can be used to encapsulate the anti-cancer drug gemcitabine and the NSID indomethacin. The highly dense fibres of the drug loaded gels are very stable and consistent with better drug incorporation. The gemcitabine-encapsulated MOG, MOG-GEM shows its anti-cancer activity. It effectively inhibits breast cancer cell proliferation even in very low dose without affecting the growth of normal fibroblast cells. The indomethacin-encapsulated MOG, MOG_IND exhibits good anti-inflammatory response against RAW 264.7 cells, suggesting this MOG could be a promising drug delivery system.

## Experimental section

### Materials

2,4-Di-*tert*-butylphenol was purchased from Sigma-Aldrich. Manganese acetate, aspartic acid and indomethacin were obtained from alfa SRL. Gemcitabine was bought from BLD pharm. Commercially available forms of formaldehyde, ethanol, and methanol was employed without additional purification. Milli Q water was used for the formation of metallohydrogel. Other common solvents of the analytical reagent grade were utilised. DMEM medium, sodium bicarbonate, antibiotic solution and FBS, propidium iodide and calcein AM were purchased from Himedia, Sigma-Aldrich, and invitrogen.

### Synthesis of metallogel and drug encapsulation

The ligand, $Na_2HL$, was synthesized by the method reported form this laboratory.[45] We first separately dissolved the ligand (0.04 equivalent, 28 mg) and $Mn(CH_3COO)_2 \cdot 4H_2O$ (0.04 equivalent, 18 mg) into 0.5 ml water. Then the ligand solution was mixed with the metal salt solution. Instant metallohydrogel formation was observed in room temperature. Inverted vial test revealed the presence of a stable gel. To prepare the indomethacin (IND) loaded gel, 5 mg IND and gelator were mixed in a solution of 1 : 1 water/ethanol and then added into the aqueous solution of $Mn^{2+}$ ion. After 10 min of standing at room temperature, we got the bulk IND loaded gel. For gemcitabine encapsulation similar method was followed, only difference is here we added the GEM into gelator solution of pure water, no ethanol was required.

### *In vitro* release GEM and IND

The experiment to validate the sustained release of the selected drug (*in vitro*) a shaker incubator having fixed speed of 50 rpm at 37 °C was employed. In a 100 ml release medium 0.6 g drug
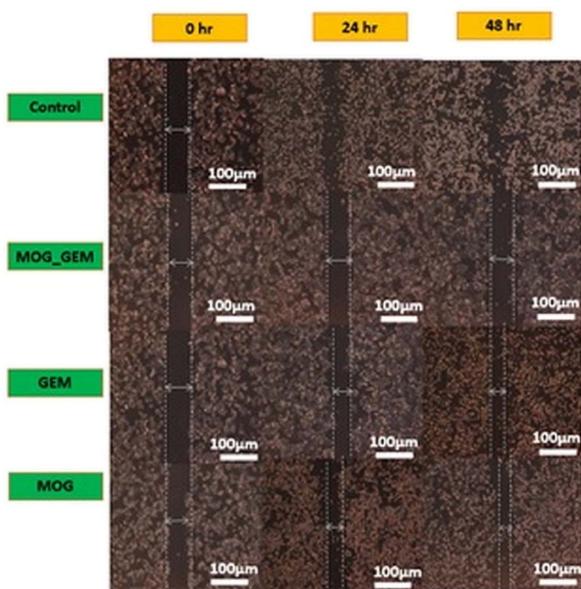


**Fig. 13** Wound healing assay of the MDA-MB-468 cell line in the treatment by MOG_GEM, GEM and MOG.

loaded gel was immersed at pH 7.4 and 5.8. At scheduled time intervals, 3 ml of solution was withdrawn and equal volume of the same dissolution medium was added back to maintain a constant volume. The amount of indomethacin and gemcitabine released from the hydrogels was determined by UV-vis spectrophotometer measurements at 318 nm and 362 nm (Shimadzu UV-160A, Japan), respectively with the help of previously calibrated standard curve. The results are the mean of two determinations.

### Cell culture

MDA-MB-468, 4T1 breast cancer cell line, RAW 264.7 mouse macrophage cell line, L929 cell lines were procured from NCCS, Pune, India. Cells were cultured in Dulbecco's Modified Eagle Medium (DMEM) with high glucose. Media was supplemented with 10% fetal bovine serum (FBS) and 1% penicillin/ streptomycin solution. Cells were maintained in humidified 37 °C, 5% $CO_2$ incubator.

### *In vitro* tumour cytotoxicity evaluation of drug incorporated MOG

MTT assay was performed to check the cell viability after treating the cells with different concentrations of the drug for 48 hours. Cells were seeded at a concentration of 8000 cells per well in 96-well MTT plate and incubated overnight. Then drug treatments of different concentrations were given to the cells except untreated control and kept for 48 h. To check the anticancer activity, we conducted the MTT assay using MOG-GEM, GEM, and MOG compounds in 4T1 and MDA-MB-468, starting at a concentration of 250 $\mu g$ $ml^{-1}$. The compounds were then serially diluted 11 times, and after 48 hours of treatment.

Next, MTT reagent was added to the cells and incubated for 3.5 hours. After that, formazan crystals were dissolved in DMSO and absorbance was measured at 595 nm using Bio-Rad iMark Microplate Absorbance Reader.

### *In vitro* cellular biocompatibility

To assess the cytocompatibility of MOG-GEM for its chemotherapeutics use, L929 cell lines were employed. MTT assay was performed to check the cell viability after treating the cells with different concentrations of the drug for 48 hours following above procedure.

### Live-dead assay

4T1 & MDA-MB-468 cells were seeded on the coverslip and kept in 4 different 35 mm plates for different treatment condition. Cells were incubated for 6 hours for attachment. Then, the plates were filled with complete Dulbecco's Modified Eagle Medium (DMEM) and incubated overnight. Next, cells were treated with MOG_GEM, GEM, and MOG, respectively except for untreated control. After 48 hours of incubation, complete DMEM media was discarded and incomplete DMEM media containing calcein AM and propidium iodide stain was added and incubated at 37 °C for 40 minutes. Then, the number of live and dead cells were observed under the fluorescent microscope.

### Cell migration assay

The scratch assay or the wound healing assay was done to determine the migratory potential of the MDA-MB-468 cells. The cells were seeded in 12 different 35 mm plates and upon attaining ~70% confluency, the plate was scratched in the middle with a pipette tip. The cell debris and dislodged cells were removed by PBS wash. Images were taken at 0, 24, and 48 hours time interval under an inverted phase-contrast microscope (Leica Microsystems, Germany).

### MALDI-TOF

MALDI-TOF spectrum of the MOG was recorded on the Bruker Daltonics Ultraflextreme equipment. A very diluted spot of metallohydrogel was mixed with 2,5-dihydroxybenzoic acid matrix and dried for a period before recording the spectra.

### Morphological studies

The morphologies of the MOG and the drug-loaded MOGs were determined by TEM, FESEM, and AFM. TEM images were recorded on analytical TEM (FEI. TECNAIG220S-TWIN) over a carbon-coated Cu (300 mesh) TEM grid. A little amount of gel was placed on the TEM grid and allowed to dry under vacuum.

The FESEM images were recorded on Zeiss EVO 60 with Oxford EDS detector operating at 5–10 kV. The sample for FESEM was prepared by smearing a small portion gel on an aluminium plate. Then the aluminium plate was dried under vacuum at room temperature for one 24 hours. Next dry gels sample were coated with gold before imaging to avoid the charging of the samples using an accelerating voltage of 50–100 kV without staining.

The AFM images were recorded on Agilent 5500 microscope. A little amount of gel was applied to a glass slit to prepare the sample for AFM. The sample was dried for a day under vacuum at room temperature. AFM images were recorded at a 100 kV accelerating voltage without being stained. All the images were taken under atmospheric conditions.

### PXRD

A Siemens D-5000 X-ray diffractometer was used to conduct the XRD experiments. The source was a DRX ceramic tube (Cu K = 1.540 560 and Cu K 2 = 1.544 390), which had a 45 kV and 35 mA voltage and current, respectively. The gel was put on a glass slide, dried, and scanned between $2\theta = 5$ to $2\theta = 90°$ with a frequency 3° per minute.

### Rheological studies

The mechanical strength and viscoelastic parameter of the gels prepared were measured using Anton Paar Physical MCR 301 Rheometer. The experiment was carried out at room temperature using newly made gel in its natural state. A 25 mm parallel plate with a genuine gap of 1 mm was used for the oscillation test. 1% strain and a frequency range of 1–100 rad $s^{-1}$ were used to quantify the dynamic frequency sweep. The shear strain range for the amplitude sweep was between 0.1 and 1000 Pa, and the angular frequency was fixed at 10 rad $s^{-1}$. The following

settings were made for the dynamic time sweep: fixed frequency: 1 Hz; shear force was applied alternatively at 0.1% at 0–100 s and 100% at 100–200 s up to 7 cycles, and the operation was subsequently repeated up to 6 cycles. Both the viscoelastic moduli are defined as follows: $G' = \tau_0/\gamma_0 \cos\delta$ and $G'' = \tau_0/\gamma_0 \sin\delta$ (where $\tau_0$ and $\gamma_0$ are the amplitudes of stress and strain).

### FT-IR

The IR spectra of dry gels were obtained with the spectrometer PerkinElmer Spectrum. On FT-IR, energy range: 450–4000 cm$^{-1}$ using the universal attenuated total reflectance accessory (U-ATR).

## Author contributions

MB planned the work. MD carried out the synthesis and characterization of the gel and study of drug release. The biological work was carried out in MM's laboratory by SB.

## Conflicts of interest

There is no conflict of interest.

## Acknowledgements

## Notes and references

1 H. Su, S. Zhu, M. Qu, R. Liu, G. Song and H. Zhu, *J. Phys. Chem. C*, 2019, **123**, 15685–15692.

2 M. Xu, Y. Lü, Q. Sun, K. Liu, Z. Liu and P. Sun, *Crys. Growth Des.*, 2015, **15**, 5360–5367.

3 N. Malviya, C. Sonkar, R. Ganguly and S. Mukhopadhyay, *Inorg. Chem.*, 2019, **58**, 7324–7334.

4 Y. Y. Li Sip, D. W. Fox, L. R. Shultz, M. Davy, H.-S. Chung, D.-X. Antony, Y. Jung, T. Jurca and L. Zhai, *ACS Appl. Nano Mater.*, 2021, **4**, 6045–6056.

5 A. Upadhyay, A. Narula and C. P. Rao, *ACS Appl. Bio Mater.*, 2020, **3**, 8619–8626.

6 W. Miao, L. Zhang, X. Wang, H. Cao, Q. Jin and M. Liu, *Chem.–Eur. J.*, 2013, **19**, 3029–3036.

7 Y. Qin, L. Chen, Y. Cheng, S. Yang, Y. Liu, W. Fan, L. Wang, Q. Wang, L. Zheng and Q. Cao, *ACS Appl. Bio Mater.*, 2020, **3**, 3268–3275.

8 B. Xu, *Langmuir*, 2009, **25**, 8375–8377.

9 N. M. Sangeetha and U. Maitra, *Chem. Soc. Rev.*, 2005, **34**, 821–836.

10 M. Ghorbanloo, A. Heydari and H. Yahiro, *Desalin. Water Treat.*, 2018, **115**, 106–114.

11 J. Sui, L. Wang, W. Zhao and J. Hao, *Chem. Commun.*, 2016, **52**, 6993–6996.

12 Z. Liu, H. Li, M. Zhu, Y. Huang, Z. Tang, Z. Pei, Z. Wang, Z. Shi, J. Liu, Y. Huang and C. Zhi, *Nano Energy*, 2018, **44**, 164–173.

13 J. Bae, Y. Li, J. Zhang, X. Zhou, F. Zhao, Y. Shi, J. B. Goodenough and G. Yu, *Angew. Chem., Int. Ed.*, 2018, **57**, 2096–2100.

14 Y. Yang, W. Liu, Q. Zhong, J. Zhang, B. Yao, X. Lian and H. Niu, *ACS Appl. Nano Mater.*, 2021, **4**, 4735–4745.

15 B. Zhang, X. Dong, Q. Zhou, S. Lu, X. Zhang, Y. Liao, Y. Yang and H. Wang, *Carbohydr. Polym.*, 2021, **263**, 117986.

16 J. Y. R. Silva, L. L. da Luz, F. G. M. Mauricio, I. B. Vasconcelos Alves, J. N. S. Ferro, E. Barreto, I. T. Weber, W. M. de Azevedo and S. A. Junior, *ACS Appl. Mater. Interfaces*, 2017, **9**, 16458–16465.

17 C. Kim, K. Y. Kim, J. H. Lee, J. Ahn, K. Sakurai, S. S. Lee and J. H. Jung, *ACS Appl. Mater. Interfaces*, 2017, **9**, 3799–3807.

18 G. Sathyanarayanan, M. Rodrigues, D. Limon, R. Rodriguez-Trujillo, J. Puigmarti-Luis, L. Perez-Garcia and D. B. Amabilino, *ACS Omega*, 2017, **2**, 8849–8858.

19 S. Panja, S. Ghosh and K. Ghosh, *New J. Chem.*, 2018, **42**, 6488–6497.

20 H. Wu, J. Zheng, A. L. Kjoniksen, W. Wang, Y. Zhang and J. Ma, *Adv. Mater.*, 2019, **31**, 1806204.

21 C. A. Offiler, C. D. Jones and J. W. Steed, *Chem. Commun.*, 2017, **53**, 2024–2027.

22 F. Mondino, A. Piscitello, C. Bianco, A. Gallo, A. de Folly D'Auris, T. Tosco, M. Tagliabue and R. Sethi, *Water*, 2020, **12**, 826.

23 F. Fages, *Angew. Chem., Int. Ed.*, 2006, **45**, 1680–1682.

24 M. O. Piepenbrock, N. Clarke and J. W. Steed, *Langmuir*, 2009, **25**, 8451–8456.

25 J. Zhang and C.-Y. Su, *Coord. Chem. Rev.*, 2013, **257**, 1373–1408.

26 J. Shen, W. Zhang, R. Qi, Z. W. Mao and H. Shen, *Chem. Soc. Rev.*, 2018, **47**, 1969–1995.

27 O. Gbolahan, N. Hashemi-Sadraei, S. Yash, G. Williams, R. Ramachandran, Y.-I. Kim, R. Paluri, D. Outlaw, B. El-Rayes and L. Nabell, *Cancer Med.*, 2022, 1–11.

28 X. Qin, L. He, C. Feng, D. Fan, W. Liang, Q. Wang and J. Fang, *ACS Appl. Mater. Interfaces*, 2021, **13**, 46270–46281.

29 N. Bhattarai, J. Gunn and M. Zhang, *Adv. Drug Deliv. Rev.*, 2010, **62**, 83–99.

30 Y. H. Lin, H. F. Liang, C. K. Chung, M. C. Chen and H. W. Sung, *Biomaterials*, 2005, **26**, 2105–2113.

31 P. Choudhary, R. Gaur, D. Rambabu, A. Dhir, A. Gupta and Pooja, *ChemistrySelect*, 2021, **6**, 9139–9143.

32 S. Mukherjee, S. Mukherjee, M. A. S. Abourehab, A. Sahebkar and P. Kesharwani, *Eur. Polym. J.*, 2022, **177**, 111471.

33 M. Ebrahimian, M. Hashemi, M. Farzadnia, S. Zarei-Ghanavati and B. Malaekeh-Nikouei, *Biotechnol. Prog.*, 2022, e3278.

34 K. Sztandera, M. Gorzkiewicz and B. Klajnert-Maculewicz, *Mol. Pharm.*, 2019, **16**, 1–23.

35 C. S. Brazel and N. A. Peppas, *Eur. J. Pharm. Biopharm.*, 2000, **49**, 47–58.

36 J. Xu, S. Strandman, J. X. Zhu, J. Barralet and M. Cerruti, *Biomaterials*, 2015, **37**, 395–404.

37 T. A. Seidu, P. T. Kutoka, D. O. Asante, M. A. Farooq, R. N. Alolga and W. Bo, *Pharmaceutics*, 2022, **14**, 1113.

38 E. Bellido, T. Hidalgo, M. V. Lozano, M. Guillevic, R. Simón-Vázquez, M. J. Santander-Ortega, Á. González-Fernández, C. Serre, M. J. Alonso and P. Horcajada, *Adv. Healthcare Mater.*, 2015, **4**, 1246–1257.

39 D. J. Levine, T. Runcevski, M. T. Kapelewski, B. K. Keitz, J. Oktawiec, D. A. Reed, J. A. Mason, H. Z. Jiang, K. A. Colwell, C. M. Legendre, S. A. FitzGerald and J. R. Long, *J. Am. Chem. Soc.*, 2016, **138**, 10143–10150.

40 K. Sarkar, S. Khasimbi, S. Mandal and P. Dastidar, *ACS Appl. Mater. Interfaces*, 2018, **10**, 30649–30661.

41 N. Malviya, C. Sonkar, R. Ganguly, D. Bhattacherjee and K. P. Bhabak, *ACS Appl. Mater. Interfaces*, 2019, **11**, 47606–47618.

42 K. Sarkar, H. K. Datta, S. Ahmed and P. Dastidar, *ChemistrySelect*, 2021, **6**, 13992–14004.

43 (*a*) C. K. Karan and M. Bhattacharjee, *Eur. J. Inorg. Chem.*, 2019, 3605–3611; (*b*) C. K. Karan, S. Mallick, C. R. Raj and M. Bhattacharjee, *Chem.–Eur. J.*, 2019, **25**, 14775–14779; (*c*) M. Dutta, C. K. Karan and M. Bhattacharjee, *ChemistrySelect*, 2022, **7**, e202203214.

44 (*a*) C. K. Karan and M. Bhattacharjee, *ACS Appl. Mater. Interfaces*, 2016, **8**, 5526–5535; (*b*) C. K. Karan, M. C. Sau and M. Bhattacharjee, *Chem. Commun.*, 2017, **53**, 1526–1529.

45 S. Dasgupta, S. Atta, N. D. P. Singh, D. Deb, W. S. Kassel and M. Bhattacharjee, *Eur. J. Inorg. Chem.*, 2014, **30**, 5125–5134.

46 Y. Li, C. W. Wei, X. J. Wang, S. Q. Gao and Y. W. Lin, *Spectrochim. Acta, Part A*, 2022, **271**, 120901.

47 S. Bhowal, A. Ghosh, S. P. Chowdhuri, R. Mondal and B. B Das, *Dalton Trans.*, 2018, **47**, 6557–6569.

48 T. Shukla, S. P. Pandey and U. K. Patil, *Indian J. Pharm. Educ. Res.*, 2014, **48**, 41–47.

49 M. Chandira, B. Jayakar, D. Bhowmik and K. S Kumar, *Int. J. Pharm. Technol.*, 2020, **2**, 23–36.

50 M. S. Amir Faiz, C. A. Che Azurahanim, S. A. Raba'ah and M. Z Ruzniza, *Results Phys.*, 2020, **16**, 102954.

51 R. Maity, S. Hohloch, C. Su, M. van der Meer and B. Sarkar, *Chem.–Eur. J.*, 2014, **20**, 9952–9961.

52 J. Li and D. J. Mooney, *Nat. Rev. Mater.*, 2016, **1**, 16071.

53 S. J. Buwalda, K. W. Boere, P. J. Dijkstra, J. Feijen, T. Vermonden and W. E. Hennink, *J. Controlled Release*, 2014, **190**, 254–273.

54 A. M. Rosales and K. S. Unseth, *Nat. Rev. Mater.*, 2016, (1), 1–15.